Defect-assisted photocatalytic activity of glass-embedded gallium oxide nanocrystals

Roberto Lorenzi[1*], Nikita V. Golubev[2], Elena S. Ignat'eva[2], Vladimir N. Sigaev[2], Chiara Ferrara[1], Maurizio Acciarri[1], Giovanni Maria Vanacore[1], Alberto Paleari[1]

[1]Department of Materials Science, University of Milano-Bicocca, via Cozzi 55, 20125 Milano, Italy
[2]P.D. Sarkisov International Laboratory of Glass-based Functional Materials, Mendeleev University of Chemical Technology of Russia, Miusskaya Square 9, 125047 Moscow, Russia
*corresponding author: roberto.lorenzi@mater.unimib.it, tel. +390264485221, fax +390264485400

Abstract

The use of glassceramics in photocatalysis is an attractive option for the realization of smart optical fibers and self-cleaning windows. Here we present the photocatalytic activity of germanosilicate glasses embedding Ga_2O_3 nanocrystals prepared by batch melting and glass heat treatment. The powdered material is used for UV-assisted degradation of rhodamine in water. The kinetics show changes after repeated experiments. In the first cycle, the apparent rate is governed by a second-order reaction with a Gaussian-like shape, whereas the second cycle follows a first-order reaction. The modification appears to be correlated with perturbations in the defect population. Photoluminescence has been used to monitor the evolution of such defects. Kinetic data on photoreactions and defect formation have been modelled in a combined frame in which the defect concentration determines the photocatalytic activity. The results prove the photocatalytic ability of the studied glassceramics. Moreover, the general validity of the kinetic model can be of interest for other systems in which the photocatalytic response depends on photoreactive species concentration.

Keywords: Glassceramics; Gallium oxide; Photocatalysis; Gaussian kinetic; Photoluminescence

Graphical Abstract

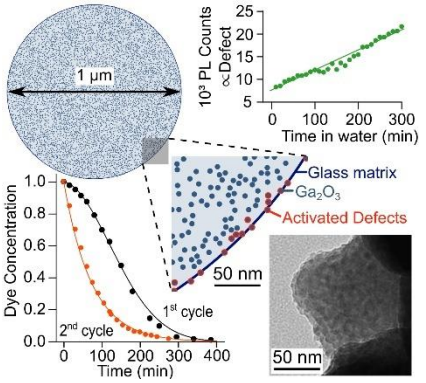

Introduction

The urgent need to find new solutions for environmental remediation is pushing the research on new materials specifically designed for heterogeneous photocatalysis. In this context, glassceramics represent an interesting alternative to the common approach based on supported catalysts.[1] In these systems the active nanoparticles, usually wide-bandgap metal oxides, are uniformly distributed in a glass matrix. An apparent drawback of using glassceramics in photocatalysis is that part of the catalyst does not participate in the photoreaction due to its location inside the bulk of the glass. From another perspective, this drawback can be of great advantage in some applications. The matrix has the same chemical durability, mechanical strength, and workability as the parent glasses. These aspects could be relevant for photocatalysis in harsh environments or unconventional geometries such as self-cleaning glasses and containers and smart optical fibers. In this view, a key requirement is the transparency of the samples which can be targeted by appropriate control of nanoparticle size and dispersion. In the last years the possibility of approaching photocatalysis by using glassceramics is attracting attention and their application on light-assisted H_2 production,[2, 3] pollutant degradation,[4, 5] and antibacterial properties[6, 7] have been proved. Much of the works regard bulk nanoprecipitation of TiO_2,[4, 8] ZnO,[6] ferroelectric oxides,[9, 10] and quantum dots[11, 12] dispersed in a transparent inorganic oxide glass matrix. Similar methods, even if the transparency of the material and the full passivation of the catalyst are not guaranteed, include surface crystallized glassceramics[13] —where only a thin top layer of the glass is opportunely treated to obtain metal oxide crystals— and active nanoparticles supported in solgel derived matrix with large surface area and porous structures.[14] Among the many transparent glassceramics accessible through conventional melt-quenching technique there is the class of gallate spinels.[15, 16] In these systems, the matrix is a mixed alkali alumino- or germano- silicate glass and the nanophase is a gallate spinel such as $LiGa_5O_8$ or the defect spinel γ-Ga_2O_3.[17, 18] The latter is a wide bandgap semiconductor (E_{GAP} of ≈4.5 eV),[19] typically obtained from mild reactions[20-25] and often in the form of nanoparticles[26] or porous structures[27], which have shown promising properties in photocatalysis.[25, 28-30] Aim of this study is to collect the necessary experimental basis for evaluating and interpreting the photocatalytic activity of transparent germanosilicate glassceramics containing nanoparticles of γ-Ga_2O_3. These materials have been deeply investigated in the last few years for their optical properties, both as regard their strong UV-excited blue luminescence from intrinsic defects and as a host for optically active ions.[31-35] Their production consists in two main steps: batch melting of the mixed starting ingredients at about 1500 °C and an opportune thermal treatment to induce nucleation and precipitation of spinel nanophase in the range 560-700 °C. The obtained materials have the same forming ability as glasses and can be processed into different geometries such as optical fibers[36] or sputtered thin films.[37] Optimized synthesis leads to nanoparticles of 4-10 nm in size with a molar concentration up to

≈20%.[38] The present work is focused on the analysis and interpretation of results of UV-assisted degradation of rhodamine to have a basis for a reliable evaluation of Ga_2O_3 as an effective photocatalyst even if confined in a glass matrix, and to give a model for the observed photocatalytic kinetics.

Materials and methods

Material Synthesis

The starting glass, with molar composition $7.5Li_2O–2.5Na_2O–20Ga_2O_3–25SiO_2–45GeO_2$, was prepared by a conventional batch melting technique and using, as raw powdered materials, amorphous SiO_2 (Ltd"Lanthan center for technology", Moscow, Russia, special purity grade), GeO_2 (JSC"Germanium", Krasnoyarsk, Russia, special purity), Li_2CO_3 (Ltd"Rare Metals Plant", Koltsovo, Russia, reagent grade), Na_2CO_3 (Ltd"JSCReachem", Moscow, Russia, reagent grade), and Ga_2O_3 (Ltd"Rare Metals Plant", Koltsovo, Russia, reagent grade). Batches were prepared by mixing carefully in an agate mortar a total of 70 g of raw materials, weighted with an analytical balance with an accuracy of 1 mg. The powders were then transferred in a ≈45 mL crucible and heated in air at 1500 °C for 60 min. The resulting melt was rapidly cooled on stainless steel plates and pressed with another steel plate obtaining amorphous glass samples. Finally, the glasses underwent further thermal treatment comprising a nucleation treatment at 570 °C for 18 h followed by nanocrystallization treatment at 651 °C for 30 min, using a muffle with temperature control of ±2 °C and a heating rate of 10 °C/min. Between the two steps, the sample was cooled down to ambient temperature by quickly removing it from the muffle. Finally, glass-ceramics were milled for 1 h in a SPEX SamplePrep 8000M mixer mill with vial and balls in ceramic zirconia. Glassceramic grain size distribution has been assessed by dynamic light scattering using a Malvern Instruments Nano Series Zetasizer working at 633 nm and measurement angles at 13° and 175°.

Photocatalysis experiment

Photocatalysis experiments were conducted following the degradation of either Rhodamine 6G (Sigma Aldrich, purity ≈95%) or phenol (Sigma Aldrich, purity ≥99%). About 30 mg of powder was weighted with an analytical balance and suspended in a 100 mL beaker with 50 mL of a 4 mg/L solution of rhodamine 6G in deionized water or a 15 mg/L solution of phenol in deionized water. Then the beaker was placed under an 8 W Hg lamp (Analytik Jena) operating at 254 nm at 3.5 cm from the suspension surface. The suspension was continuously stirred during the photocatalytic experiment and the dye concentration was monitored by measuring the absorbance at 527 nm with an optical fibre probe attached to a Cary 60 UV-vis spectrometer. To perform cycling tests, the powder was collected by centrifugation after complete degradation of the dye, washed three times with deionized water, and dried at 165 °C for 12 h.

Time resolved photoluminescence

Time resolved photoluminescence has been performed on powder suspensions using an Edinburgh FLS 980 spectrofluorometer equipped with a pulsed diode (EP-LED series by Edinburgh) as excitation source with a pulse duration of 600 ps and emitting at 250 nm. The signal was collected in time-correlated single photon counting mode at 450 nm and with a bandpass of 20 nm. The sample was kept under continuous stirring in a quartz cell (1 cm path length) during acquisition.

Material characterization

X-ray diffraction (XRD) patterns have been collected on a Rigaku Miniflex 600 in the angular range 20°-70° (step size 0.02°) with the use of Cu Kα radiation. Surface morphology were studied on powdered samples without any further treatment or deposition by a Gemini 500 Zeiss scanning electron microscope (SEM). Transmission electron microscope (TEM) investigations were performed at the Microscopy Platform of the University of Milano-Bicocca (Italy) using a JEOL JEM 2100P operating at 200 kV, equipped with a LaB6 source, and exhibiting a nominal point resolution of 2.4 Å. The images were then recorded with a Gatan RIO CMOS camera. The synthesized samples were dispersed in a solvent and transferred via drop casting onto a Cu grid, covered by a thin (3-4 nm) amorphous Carbon membrane. Images were taken at room temperature at different magnifications, with the TEM operated in bright-field parallel imaging mode, and adopting an in-gap objective aperture. Energy-dispersive X-ray fluorescence spectroscopy (XRF) was performed with a Bruker Artax 200 spectrometer, equipped with an X-ray tube (Mo anode) with a beam collimated down to 0.65 mm in diameter. Bruker Spectra 5.1 software was used to perform peak deconvolution.

Results and discussion

Material nanostructuring and Photocatalytic activity

The investigated glassceramic material has been produced by tailoring nanostructure size and concentration. The aim is to obtain a large number of active nanocrystals per unit volume with minimized crystal size and a large resulting active surface. These features, both relevant for a potential photocatalytic activity, can be controlled in detail thanks to previous structural, thermal, and functional properties assessments. Following the approach of Marotta et al.,[34, 39, 40] the nucleation rate and the number of crystal nuclei per unit volume are maximized when the difference between the temperatures of the exothermic peak of crystallization in the nucleation pre-treated and as-quenched untreated material is maximized. On the one hand, the total volume of the crystallized Ga_2O_3 phase is limited by the total amount of Ga in the glass composition. On the other hand, the total volume is equal to the product of the mean nanoparticle size and the number of crystal nuclei formed during the nucleation treatment. Therefore, the larger the number of crystal nuclei, the smaller the nanoparticle size. The crystallization temperature has been recorded after nucleation pre-treatments at different temperatures by differential scanning calorimetry,

finding the best nucleation and crystallization temperatures following Marotta's method. According to this approach, the material for the present photocatalytic experiments has been treated in conditions close to the maximization of the number of nuclei per unit volume and, accordingly, to the crystal size minimization. In these conditions, from the statistical analysis of transmission electron microscopy images (see Fig. S1 in Supporting information for representative TEM images), the precipitated γ-Ga_2O_3 nanocrystals turn out to have a mean diameter of 6 nm with a bimodal distribution, with maxima at 5 nm and 7 nm, the last one resulting from the coalescence of tiny crystals formed during nucleation pre-treatment.[38] Remarkably, the structural features arising from the thermal history of the sample also dictate functional optical properties which are strictly related to the potential photocatalytic activity, i.e. the photo-excitation and decay channels of the nanophase. The prepared material shows enhanced intrinsic photoluminescence activity as compared to other samples with the same composition but thermally treated in different ways.[38] This outcome is the result of two concomitant effects: a larger number of nanoparticles and a suitable occurrence of intrinsic defects.[41] The blue luminescence of Ga_2O_3 indeed arises from radiative recombination, upon band-to-band excitation, of donor-acceptor pairs where the donor is an oxygen vacancy while the acceptor is a complex of oxygen and gallium vacancies.[41] These defects can play a crucial role in photocatalysis since the first steps of photoreactions involve the trapping of holes and electrons at defect sites.[42] Indeed, the results in Fig. 1 demonstrate the ability of the glassceramic material to photodegrade rhodamine and others no-dye organic compound (Fig. S2 in Supporting Information on photodegradation of phenol). The absorption spectrum of 50 mL dye suspension with 32 mg of glassceramics, reported in Fig. 1a, gradually attenuates with time becoming undetectable in about 6 hours. The photocatalytic kinetics, reported in Fig. 1b, have been evaluated by plotting $C(t)/C_0$, where C_0 and $C(t)$ are the initial dye concentration and the concentration after a time t, respectively. Their values have been calculated using the Bouguer-Lambert-Beer relation and considering dye concentration proportional to the registered absorbance at dye absorption maximum at 527 nm. A first evident but important result on the glassceramic photocatalytic mechanism – red triangles in Fig. 1b – is that nanoparticles truly participate in the photoreaction. In fact, performing the same experiment on parent glass with equal composition – green squares in Fig. 1b – does not show any significant variation in the dye concentration, even after 7 hours of UV irradiation. Notably, the only difference between parent glass and treated glassceramics relies on the nanostructuring triggered by their thermal history. Although it has been proved that also in the glass there is partial segregation of Ga-rich phases of the order of a few nanometers in size,[31] such inhomogeneities do not have an appropriate electronic band structure to give rise to electron-hole pair generation. Conversely, this situation occurs when γ-Ga_2O_3 phase precipitates inside the glass and its photocatalytic activity can be exploited even if a large part of the nanocrystals remains inside the micro-grains of powdered glassceramics and is not in direct contact with the dye solution.

In the light of the above, some noteworthy considerations can be made from the comparison with free-standing γ-Ga_2O_3 nanoparticles used in photocatalysis.[30] The main distinction regards the law describing the kinetic which, in general, for metal oxide nanoparticles relies on 1st order rate (i.e., a straight line in semi-log plot) which approximates the model.[43] For glassceramics we observe instead a more complex behavior which will be analyzed in detail in the next section. A quantitative evaluation of the photocatalytic activity can be obtained from the comparison with a reference sample of commercial titanium oxide (1.2 mg of P25 by Degussa), black circles in Fig. 1b. In this case, the reaction follows a 1st order kinetic and it is governed by a simple exponential law of the form $C(t)=C_0\ Exp(-k\ t)$, with a measured rate constant k of 0.054 min^{-1}. For glassceramics, it is not possible to calculate a rate constant over the entire time range. Rather, we can estimate a similar figure of merit given from the apparent rate at which the initial concentration drops by a factor e, which results to be 0.0059 min^{-1}. Starting from the values of the two rate constants and normalizing for the powder mass, we have a rate of $4.5\cdot10^{-2}$ min^{-1} mg^{-1} and $1.8\cdot10^{-4}$ min^{-1} mg^{-1} for P25 and glassceramics, respectively. An analogous calculation can be done starting from literature rate constants collected on similar photocatalytic experiments on free-standing γ-Ga_2O_3 nanoparticles. The two values are $1.4\cdot10^{-2}$ min^{-1} mg^{-1} and $5.0\cdot10^{-4}$ min^{-1} mg^{-1} for P25 and γ-Ga_2O_3, respectively.[44] We highlight that it is not possible to directly compare the constant rates obtained in different experimental setups mainly because of the different illumination geometries. Instead, we can compare the ratio of the constant rates, for each experiment, and use P25 as common reference standard. As a result, in our experiments, the glassceramic material is about 250 times slower compared to P25, while the same ratio is equal to ≈30 for pure γ-Ga_2O_3 powder. This result is surprising if we consider the different volumes and exposed total area of active nanophase in the case of free nanopowders and glass-incorporated nanoparticles. From simple geometrical considerations, it is possible to estimate the fraction of embedded nanoparticles which can actively participate in the surface-mediated photocatalytic reaction. From dynamic light scattering measurements, we know that the glassceramic grains have a diameter of 930±180 nm. If we consider a glassceramic grain with a diameter d_{GC} of 1000 nm, and a volume V_{GC} = $5.2\cdot10^8$ nm^3, then the total volume occupied by the nanocrystals V_{NC} is dictated by the glassceramic composition and it is about equal to $0.2\cdot V_{GC}$, neglecting in a first approximation the difference in the molar volumes of γ-Ga_2O_3 (31 cm^3 mol^{-1})[45] and the surrounding glass (24 cm^3 mol^{-1}).[46] The total number of nanocrystals in the grain is therefore $N_{NC}=0.2V_{GC}/V_{NC}=9.2\cdot10^5$, where $V_{NC}=113\ nm^3$ is the volume of a single nanocrystal with a diameter d_{NC} of 6 nm. A similar approach can be implemented to estimate the number of nanocrystals in contact with the suspension, but in this case the total volume of glassceramics considered is a thin shell of the grain with a thickness equal to the nanocrystal diameter, i.e., a nanocrystal is at the grain surface only if its distance from the surface is less than its lateral dimension. The volume of the shell is $V_{Shell}=4/3\pi[(d_{GC}/2)^3-(d_{GC}/2-d_{NC})^3]=1.8\cdot10^7\ nm^3$ and the number of nanocrystals in the shell is $N_{NP,Shell}=0.2V_{Shell}/V_{NC}=3.3\cdot10^4$. The result of these rough estimations demonstrates that, for grains of 1 μm in size, only 3.6% of the embedded nanocrystals are expected to lie

close to the surface and to truly participate in the photoreaction. To verify the hypothesis that only the surface nanoparticles take part to the reaction, we have tested also glassceramics ball-milled for only 10 minutes and with a grain size of about 2 μm. The resulting fraction of surface nanoparticles is 1.2%, obtained from the same calculation showed before. The apparent rate constant is $3.2 \cdot 10^{-4}$ min^{-1} mg^{-1} (the kinetics is reported in Fig. S3). As expected, by halving the number of surface nanoparticles we register a doubling of the rate constants. Furthermore, the rate has been normalized by the weight of the powder and not for the net weight of Ga_2O_3 as in free-standing experiments. Therefore, we have to take into account that the amount of Ga_2O_3 nanophase which can potentially react in the suspension is the 3.6% of about 20% of the weighted glassceramic powder. This corresponds to ≈0.7% of the same amount of powder of free-standing Ga_2O_3 nanocrystals in which the 100% of the material is in contact with the suspension. Therefore, only by geometric consideration, the glassceramic system is expected to show a rate about 150 times slower. By contrast, the apparent reaction rate of the glassceramics is only 8 times slower than free-standing γ-Ga_2O_3 nanocrystals. A further confirmation of the high-performing photocatalytic activity of these glassceramics comes from direct comparison with the results obtained from commercial powder of β-Ga_2O_3 (Sigma Aldrich, purity 99.99%). By comparing the kinetics collected on the same amount of glassceramics and β-Ga_2O_3 (orange diamonds in Fig. 1b), we obtain apparent rates of $1.8 \cdot 10^{-4}$ min^{-1} mg^{-1} and $3.0 \cdot 10^{-4}$ min^{-1} mg^{-1}, respectively. The two rates are comparable, having the same order of magnitude. However we have to consider that, unlike pure β-Ga_2O_3, 30 mg of glassceramics contains only ≈6 mg of Ga_2O_3.

The role of defects

From previous argumentation, the remarkable photocatalytic performance of the glassceramic material cannot be ascribed to the synthesis-induced material nanoarchitecture alone. Metal oxide photocatalytic activity is not only the consequence of a large specific area, typical of nanostructures but also the result of fine control over defect- and surface- engineering. The same occurs for γ-Ga_2O_3 nanocrystals, where post-synthesis thermal treatments and/or codoping alter the defect population and can significantly improve photocatalytic performances.[30, 47, 48] The nature of these defects will be discussed in the next sections. However, in a first approximation and taking into account that the thermal treatments also maximize light emission,[38] we can suppose that the relevant defects are quantitatively related to the sites responsible for blue luminescence, or even ascribable to the light-emitting sites themselves. The importance and the role of defects are clarified by replicas of the photocatalytic experiments performed as cycling tests after powder recovery. The main results are summarized in Fig. 2 in which the photocatalytic performances of the second round of measurements are reported after different treatments of the powder. The first striking feature in Fig.2a is that the photoreaction of the second cycle is faster than the first one, even if the powder added to the solution was less. Another relevant difference is the change in the kinetic law which,

in the case of the second cycle, is a 1st order reaction. Before entering into the details of the observed kinetics, we can preliminary investigate the possible causes of the phenomenon. Two main physical and chemical processes could modify the glassceramics as a result of the 1st cycle: the prolonged stay in water under UV illumination and a mild thermal treatment at 165 °C overnight. Fig. 2b reports the second cycle kinetics following the application of each of the two separate processes, without UV exposure. Data are collected after leaving the powder in water for 5 hours (red dots in Fig. 2b) and after overnight heat treatment in a muffle at 165 °C (blue dots in Fig. 2b). The results demonstrate that the thermal treatment alone does not induce any appreciable change in the photocatalytic performance. Indeed, the temperatures used in powders drying are by far too low for any energy-activated re-crystallization processes or atom diffusion to promote defect reorganization. On the contrary, detectable changes in kinetics are registered after the prolonged immersion in water which acts as a modifier even without the presence of UV light. Notably, similar results are obtained by leaving the powder in suspension overnight and then performing the photodegradation experiment (Fig. S4 in Supporting information). As in the cycling experiment with rhodamine, the change regards both the kinetic law underlying the photoreaction and the reaction rate decreasing.

The role of water

Further details come from the monitoring of pH value of the suspension for 8 hours, as reported in Fig. 3a. The pH increases following two different regimes: a steeper linear increment from the initial value of 6.7 to 7.7 in about 250 min and a final plateau to a constant value, within the experimental error, of 7.8±0.1 for the rest of the experiment. The main cause of pH change is certainly due to ions exchange between the powder and the water in the suspension.[49] Due to the composite nature of glassceramics, ions leaching can be originated both by the nanoparticle or by the glass matrix. Ga_2O_3 has very high chemical stability and direct interaction with water can be excluded.[50] Germanosilicate glasses perturbed by alkali metal modifiers are instead prone to ion leaching.[51] Typically, the corrosion starts with ion-exchange reactions which consist of Na^+ and Li^+ ions leaching and the incorporation of H^+ ions. These reactions thus imply an increase in the pH of the solution. After a certain amount of time, a silica-rich film is formed due to the depletion of alkali ions. Such silica-rich film is sufficiently inert toward further reactions with waters to prevent any other leaching of ions. The extent of these modification regards only few surface layers of the glassceramics as evidenced by several control experiment conducted before and after rest in water. The general stoichiometry of the system remains unaltered by water treatment (see XRF results in Table S1). SEM images collected before and after cycling experiments, and reported in Fig. 4, do not show major differences in the morphology of the individual grains and their surfaces. Also XRD analysis (Fig. S5) does not evidence important changes neither in the broad halo originated by the amorphous matrix nor in the peaks of crystalline γ-Ga_2O_3 nanophase. Beyond ion exchanges, the reaction of complex oxide glasses with

water implies other consequences, including network relaxation as a result of hydrolysis and condensation reactions, and rearrangement of non-bridging oxygen sites.[52] This latter mechanism can impact not only the amorphous phase and it can also propagate inside the nanoparticles or at their surface. As a result, the relative population of defects – which ensure charge balance at nanoparticle level – can be altered.

The effects of this change also influence the photoluminescence response of the powdered glassceramic water suspension. These samples are characterized by strong blue emission under UV-C light. As reported in Fig. 3b, the emission spectra collected on powder excited at 250 nm shows a broad peak centered at about 450 nm. This emission is attributed to the radiative recombination of donor-acceptor pairs (DAP) created by band-to-band excitation.[53] Under UV light, electrons and holes are generated, then they are trapped by donor and acceptor sites, respectively. Eventually, if the two sites are close to each other, radiative recombination of the trapped charges can take place and give rise to the emission of a photon with energy lower than the semiconductor energy gap. The nature of the donor and the acceptor impurities is strictly related to the defectiveness of the oxide. For Ga_2O_3 the donor is a neutral oxygen vacancy V_0^x and the acceptor is a gallium–oxygen vacancy pair $(V_0,V_{Ga})'$.[41] Time resolved photoluminescence from DAP recombination in Ga_2O_3 is a very sensitive probe of possible variations in the defect population either from doping with aliovalent ions or from the change in nanoparticle size or morphology. The temporal behavior of DAP emission is quite complex and can be studied looking at very different time scales from ms to ns.[26, 54] Several models have been applied for adequately describing the underlying decay law, from hyperbolic decay to stretched exponential, depending on the details of the decay mechanism.[26, 54] In this work, just to obtain a reliable estimation of the effective lifetime throughout the photocatalysis cycling, we analyze the collected data as a sum of three exponentials. The minimum for adequately reproducing the registered decay curves. The fit includes the temporal deconvolution of the Gaussian instrument response function (IRF): $I(t)=(f\star g)(t)$, where $f(t)=\Sigma a_i Exp(-t/\tau_i)$ and $g(t)=IRF$ are the functions describing the effective lifetime and the IRF, respectively (the exact analytic expression used to fit data is reported in the Supporting Information). From the fitting result, the intensity average lifetime was used as a parameter to describe the mean lifetime of the system:

$$\langle\tau\rangle = \frac{\sum_{i=1}^{3} a_i\,\tau_i^2}{\sum_{i=1}^{3} a_i\,\tau_i} \quad Eq.1$$

This approach satisfactorily fits the experimental data avoiding possible misinterpretations of the decay mechanism. Time resolved photoluminescence has been collected on suspension of powdered glassceramics in water. As in pH monitoring experiments, data have been collected every 15 min for 300 minutes. To follow DAP recombination, we monitored the emission at 450 nm excited at 250 nm, looking at a time window of 100 ns and a corresponding excitation repetition rate of 10 MHz. The results collected at the beginning (t=0 min) and the end (t=300 min) of the experiment are shown in Fig. 3c. Importantly, Fig. 3c

reports raw data without applying any baseline correction or normalization. It is worth noting that the measured background is only minimally caused by unwanted noise since the dark signal collected in the same condition is about 30 counts. The observed background of 90 and 180 counts at t=0 min and t=300 min, respectively, is mostly due to tails from slower decays in the microsecond domain that are recorded as a constant background. Accordingly, also the background has a physical meaning, and it can be considered as a true signal resulting from DAP recombination. Beyond the background intensity, also the net peak height is increasing with time, passing from 400 to 600 counts. The detailed analysis of the intensity rate growth is discussed in the next section, also considering its role in the photodegradation reactions. The increment of PL counts indicates either the occurrence of suppression of non-radiative decay channels or an effective increase of defect population or both. To examine in some detail the role of these two contributions, we must consider the photoluminescence kinetics. The ratio between radiative and non-radiative decay channels also affects the photoluminescence mean lifetime. The mean lifetime can be expressed as $\langle\tau\rangle=1/(k_r+k_{nr})$, where k_r and k_{nr} are the radiative and non-radiative rates, respectively.[55] A suppression of non-radiative decay channels thus leads to a slowdown of decay. In the inset of Fig. 3c, normalized time-resolved data are reported together with *IRF* and a slowdown of decay after long exposure in water is indeed registered. Fig. 3d reports the results of the fitted average lifetime (the complete table with fitting results is reported in Table S2), showing a monotonic increase and doubling its initial value of 8.2 ns to 16.3 ns after 300 minutes in water. Indeed, our results on photoluminescence lifetime confirm that the interaction of glassceramics with water suppresses non-radiative decay channels through the rearrangement of point defects. Moreover, since photoluminescence data are collected in fixed experimental geometry, the signal is proportional to the quantum yield – the ratio between emitted and absorbed photons – of the system because the solid angle of the collection remains unchanged during the experiment. The collected signal will be $I= K_{Geo}NQ$, where K_{Geo}, N, and Q are the geometric/instrumental factor, the number of emitting species excited by the source, and the quantum yield, respectively. The quantum yield of luminescence is in turn related to the radiative and non-radiative rates: $Q=k_r/(k_r+k_{nr})=k_r\langle\tau\rangle$.[55] If now we consider that τ_{Nat} the natural lifetime of the system – the lifetime without non-radiative decay channels – is intrinsic of the emitting species, then it is expected that $\tau_{Nat}=1/k_r=\langle\tau\rangle/Q$ is a constant independent of the amount of non-radiative decay channels. Thus, the ratio $\langle\tau\rangle/I=\langle\tau\rangle/K_{Geo}NQ$ is inversely proportional to the number of emitting sites and it is constant if and only if the number of emitting species remains fixed. On the contrary, we observe a decrease of $\langle\tau\rangle/I$ (see Fig. S7 Supporting Info) as the glass-ceramic powder remains in the water. Hence, from the photoluminescence experiment, we can conclude that the effects of water comprise both an increase of the number of DAP species and the suppression of non-radiative paths. Interestingly, a strict correlation between DAP emission in Ga_2O_3 and photocatalytic activity has already been described.[30] A decrease of the rate constant of photocatalysis is accompanied by a decrease of the average lifetime of the blue luminescence and vice versa. A long-living

DAP recombination process is indicative of a system able to efficiently capture electrons and holes through trapping by native defects in the oxide. These trapped and well-separated charges are then readily available to initiate the photocatalytic process.

Kinetic model

Given the outcomes of the previous experiments, we can trace out a kinetic model aimed at a unified description of the cycling photocatalytic experiments and the evolution of the defect population. The common model used in heterogeneous catalysis of metal oxides is the Langmuir-Hinshelwood model:

$$-\frac{dC(t)}{dt} = k_{ph}\theta = k_{ph}\frac{KC(t)}{1+KC(t)} \quad Eq.2$$

where the rate is proportional to the product of the photocatalytic rate, k_{ph}, and the fractional occupancy of the adsorption sites θ, which, in turn, depends on the adsorption rate *K* and the dye concentration *C*. Although the differential equation of the Langmuir-Hinshelwood model admits a solution of the form:

$$C(t) = \frac{\mathrm{W}\left[KC_0 e^{\mathrm{K}(C_0+k_{ph}t)}\right]}{\mathrm{K}} \quad Eq.\ 3$$

where *W* represents the Lambert W function; in the context of photocatalysis Eq. 3 is rarely applied and the preferred model assumes a small value of *KC* and, consequently, θ≈*KC*.[56] Using this approximation, Eq. 2 becomes a first-order reaction equation with an apparent rate $k_{app}=k_{ph}K$ with a simple exponential solution $C=C_0Exp[-k_{app}t]$. Hence, the latter results are the typical approach used in the description of heterogeneous catalysis. Indeed, looking at our results, such an approximation appears valid in the case of the cycled powder, in which we register first-order kinetics. Conversely, the Langmuir-Hinshelwood model does not apply to the kinetics of the pristine powder neither using Eq. 3 nor its approximation. To develop an ad hoc model, we must consider the role of defects in photocatalysis and the growth of their number due to the interaction with water. This situation can be described by a simple rate equation in which the photocatalysis reaction rate depends on the concentrations of the two involved species, i.e. the dye and the defects:

$$-\frac{dC(t)}{dt} = k_{ph}C(t)C_D(t) \quad Eq.4$$

A hint about the temporal evolution of the defect concentration, $C_D(t)$, comes from the photoluminescence experiment. The observed growth of photoluminescence intensity is linear (Fig. 5a), thus we can assume a zero-order kinetic reaction for $C_D(t)$:

$$\frac{dC_D(t)}{dt} = k_D \quad Eq.5$$

As regards k_{ph}, the data collected in the second cycle allow us to obtain an evaluation. The defect population does not change any more during the second cycle, as confirmed by pH study, while the photocatalytic activity is only governed by the dye concentration:

$$-\frac{dC(t)}{dt} = k_{ph}C(t) \quad Eq.6$$

Importantly, the proposed model is not in contradiction with the Langmuir-Hinshelwood model. Rather, the main difference between these kinetics and more usual photocatalytic reactions relies on the rate-determining step of the reactions. In the Langmuir-Hinshelwood model is the number of adsorbed sites that play the main role in the photocatalytic process. In the present model, this role is not played by the adsorbed sites themselves, but by the formation and then the stabilized occurrence of active defects in the proximity of the same sites. Here, we have neglected the adsorption step and we have implicitly assumed that the adsorption rate is orders of magnitude lower than the defect creation rate. Alternatively, the photocatalytic rate k_{ph}, as in the reduced Langmuir-Hinshelwood model, can be thought of as an apparent rate that accounts for both the photocatalytic and the adsorption rates. Summarizing the differential equations, we have:

$$\begin{array}{cc} 1st\ cycle & -\frac{dC(t)}{dt} = k_{ph}C(t)C_D(t) \\ Defect\ growth & \frac{dC_D(t)}{dt} = k_D \\ 2nd\ cycle & -\frac{dC(t)}{dt} = k_{ph}C(t) \end{array} \quad Eq.7$$

This system of equations admits the following solution, where C_{D0} is the defect concentration at time t=0:

$$\begin{array}{cc} 1st\ cycle & C(t) = C_0 e^{-k_{ph}t\left(C_{D0}+\frac{1}{2}k_D t\right)} \\ Defect\ growth & C_D(t) = C_{D0} + k_D t \\ 2nd\ cycle & C(t) = C_0\, e^{-k_{ph}t} \end{array} \quad Eq.8$$

Before applying this model to our results, we have to make some important comments. First, the equation describing the 1st cycle experiment is a bell-shaped function. In the case of $C_{D0}=0$, it corresponds to a Gaussian function of the type $exp[-a\ t^2]$ defined only for positive t, centered at $t=0$, and a width, in terms of standard deviation, of $(k_D k_{Ph})^{-1/2}$. The use of Gaussian functions for photocatalytic kinetics of metal oxides has been already used, although in those works their use is based on empirical observations rather than on a kinetic model.[57, 58] Second, the analytical expression describing the defects evolution considers only those defects which actively participate to the photocatalytic process. Data reported in Fig. 5a are instead the result of photoluminescence experiments which probe all the light-emitting defects in the sample. Accordingly, data fitting cannot neglect two facts: 1) we must distinguish between the defects in nanoparticles at the surface of the glassceramic grains and all the other defects (in nanoparticles within the

bulk of the grains), and 2) photoluminescence counts are proportional to the number of defects, but cannot be converted in a quantitative evaluation of the concentration C_D of the defects. Because of the abovementioned caveat and normalizing data for the dye concentration at t=0, we obtain a set of three equations that fit the set of our photoluminescence experiment (red lines in Fig. 5):

$$\begin{array}{cc} 1st\ cycle & C(t) = e^{-k_{ph}t\left(C_{D0}+\frac{1}{2}k_D t\right)} \\ Defect & C_D(t) = c_{PL}(C_{Bulk} + C_{D0} + k_D t) \\ 2nd\ cycle & C(t) = e^{-k_{ph}t} \end{array} \quad Eq.9$$

Here we have introduced the conversion factor c_{PL} from photoluminescence counts to defect concentration and the concentration C_{Bulk} of the defects affecting nanoparticles located inside the glassceramic grain. Importantly, data fitting is the result of simultaneous analysis of all data throughout the cycling experiments (red lines in Fig. 5 and Tab. S2 Supporting Info), thus the common parameters k_{ph}, C_{D0}, and k_D are constrained to assume the same value in the simultaneous fit of the three equations. As expected, the results confirm that the value of k_{ph} is $1.3 \cdot 10^{-2}$ min^{-1} while the k_D is $4.8 \cdot 10^{-3}$ min^{-1}, suggesting that the formation of defects is about 3 times slower than the effective photoreaction rate. More interestingly, the ratio $C_{D0}/(C_{D0}+C_{Bulk})$, which represents the fraction of defects at the nanoparticle surface over the total number of defects, is 3.9%. This outcome is strikingly close to the value of 3.6% calculated from geometrical considerations. These two main points– the rate of defect formation as a limiting factor of the observed kinetics and the agreement between the two independent evaluations of the fraction of surface defects – strongly support the proposed analysis of the photocatalytic activity of the present system.

Conclusion

In summary, we have investigated the photocatalytic performances of micrometric glassceramic powders in which nanocrystals of Ga_2O_3 are finely dispersed in a germanosilicate matrix. Despite the encapsulation in a glass host, the observed rhodamine degradation rates under UV light are comparable to those registered for free-standing Ga_2O_3. Cycling experiments on recovered glassceramic powder have shown both a boosting on the photocatalytic performances and a change in the reaction order which passes from a Gaussian-like second-order reaction to a first-order reaction as expected from the Langmuir-Hinshelwood theory. The origin of these effects has been attributed to the matrix modifications induced by the chemical interactions between water and glassceramics. The leakage of alkali elements from the glass matrix modifies the population of native defects in the glassceramics which eventually increases the number of defects at the surface of the nanoparticles. The latter is crucial for the photocatalytic activity of gallium oxide as well as for its strong luminescence intensity which grows linearly with the time that the glassceramic spends in the water. Finally, we have successfully modelled a unified system of equation rates which can describe the Gaussian-like shape of photoreaction kinetics of the pristine material, the first-order photoreaction rate of the recovered powder, and the zero-order reaction of the photoluminescence

kinetics. As expected, the results suggest that only those defects belonging to nanoparticles at the surface of the glassceramic grains actively participate in the rhodamine degradation and their formation is the rate-limiting step of the photocatalytic activity.

Acknowledgements

Financial support from the Italian Ministry of University and Research (MIUR) through grant ‘‘Dipartimenti di Eccellenza-2017 Materials for Energy’’, University of Milano-Bicocca through grant ‘‘Bando Infrastrutture di Ricerca – Edizione 2021’’ and Mendeleev University of Chemical Technology of Russia (Project Number 2020-036) are gratefully acknowledged. The authors gratefully thank Dario Bertuzzi, Beatrice Trovò, and Costanza Baldacconi from University of Milano-Bicocca, and Dr. Alberto Bianchi from Graftonica S.r.L for their help in collecting part of the experimental data.

Figures

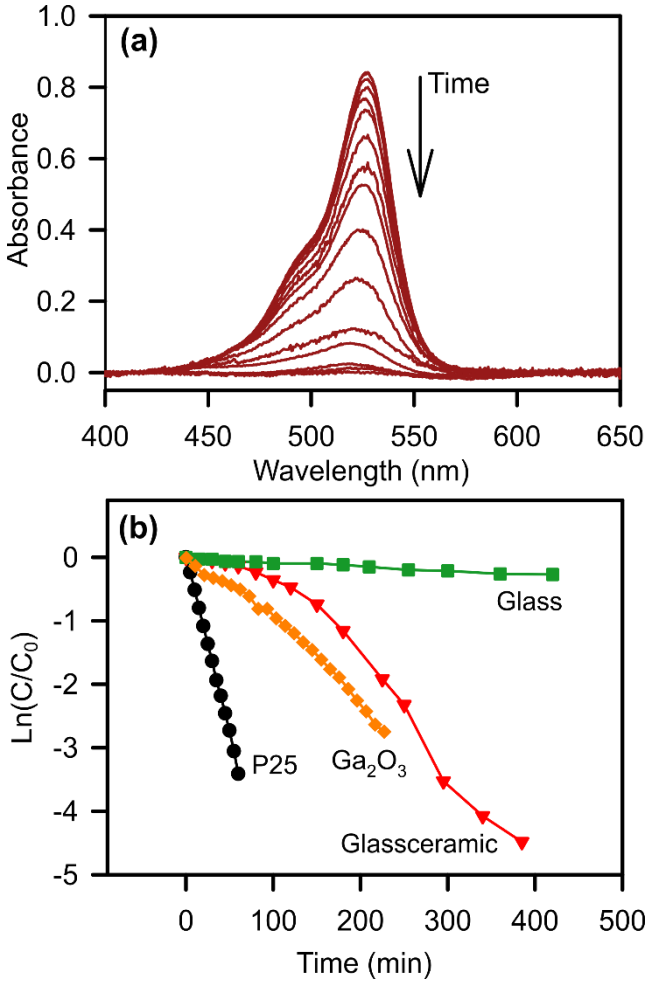

Figure 1: (a) Absorption spectra of a suspension of ≈30 mg of powdered glassceramic and Rhodamine 6G during photocatalytic experiment. (b) Rhodamine absorption maxima as a function of UV exposure for glassceramic (red triangles), glass (green squares), pure commercial gallium oxide (orange diamonds), and commercial TiO_2 P25 (black circles). The curves are normalized for the value at t=0.

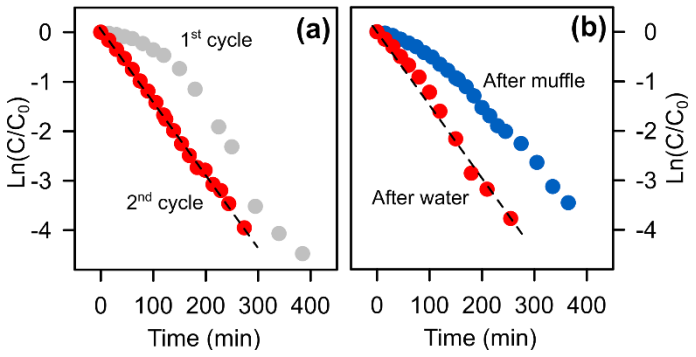

Figure 2: (a) Cycling photocatalytic kinetics before (grey points) and after (red points) recovery of glassceramic powders and (b) photocatalytic kinetics of powdered glassceramic after 5 h in water (red points) and after overnight treatment at 165 °C (blue points).

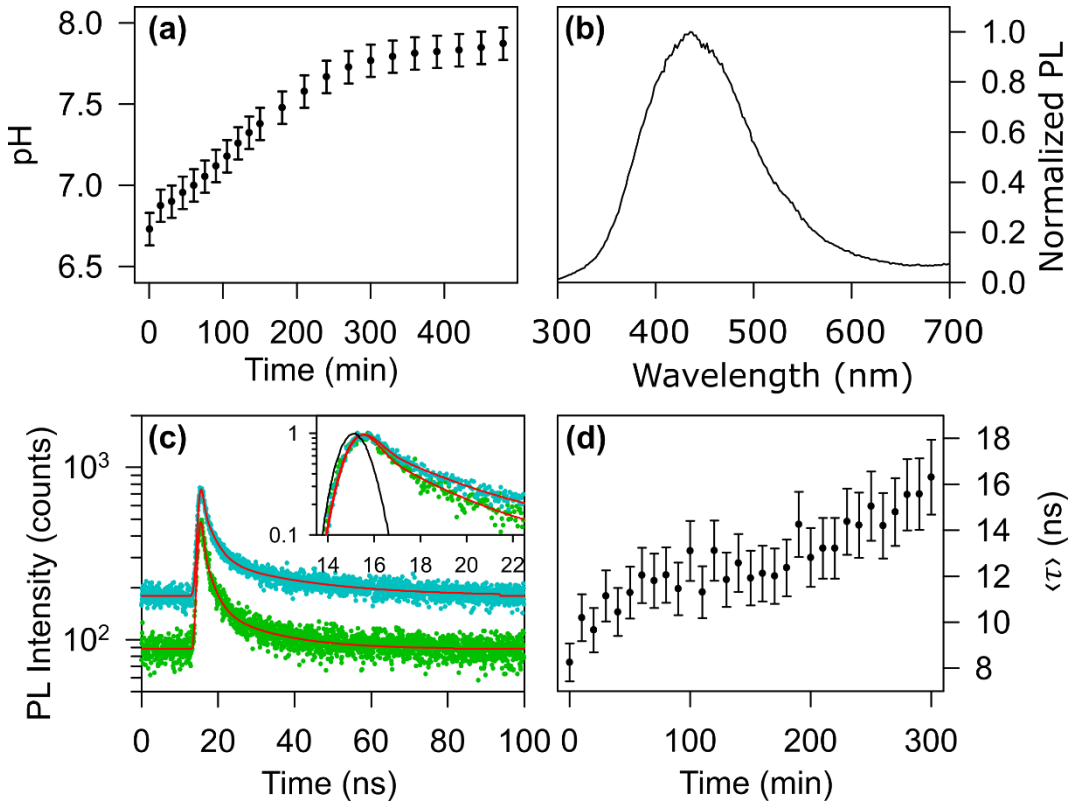

Figure 3: (a) pH evolution of an aqueous suspension of powdered glassceramic. (b) Photoluminescence spectrum of the glassceramics with excitation at 250 nm. (c) Raw time-resolved photoluminescence profile excited a t 250 nm and monitored at 450 nm of an as-prepared glassceramic suspension (green dots) and after 300 min (blue dots) with their fitting curves (red lines), in the inset the same data after normalization, the Instrument Response Function is represented by a black solid line. (d) Mean photoluminescence lifetime of glassceramic suspension as a function of time.

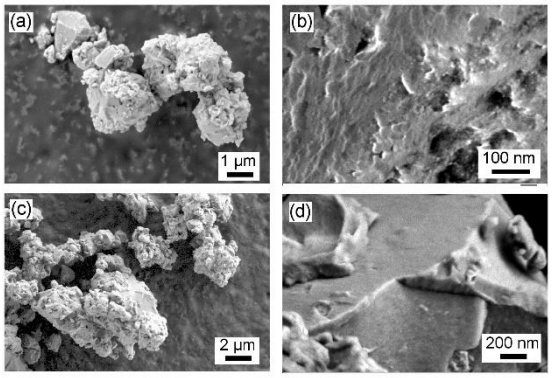

Figure 4: SEM images of powdered glassceramics before (a and b) and after (c and d) rest in water for 6h.

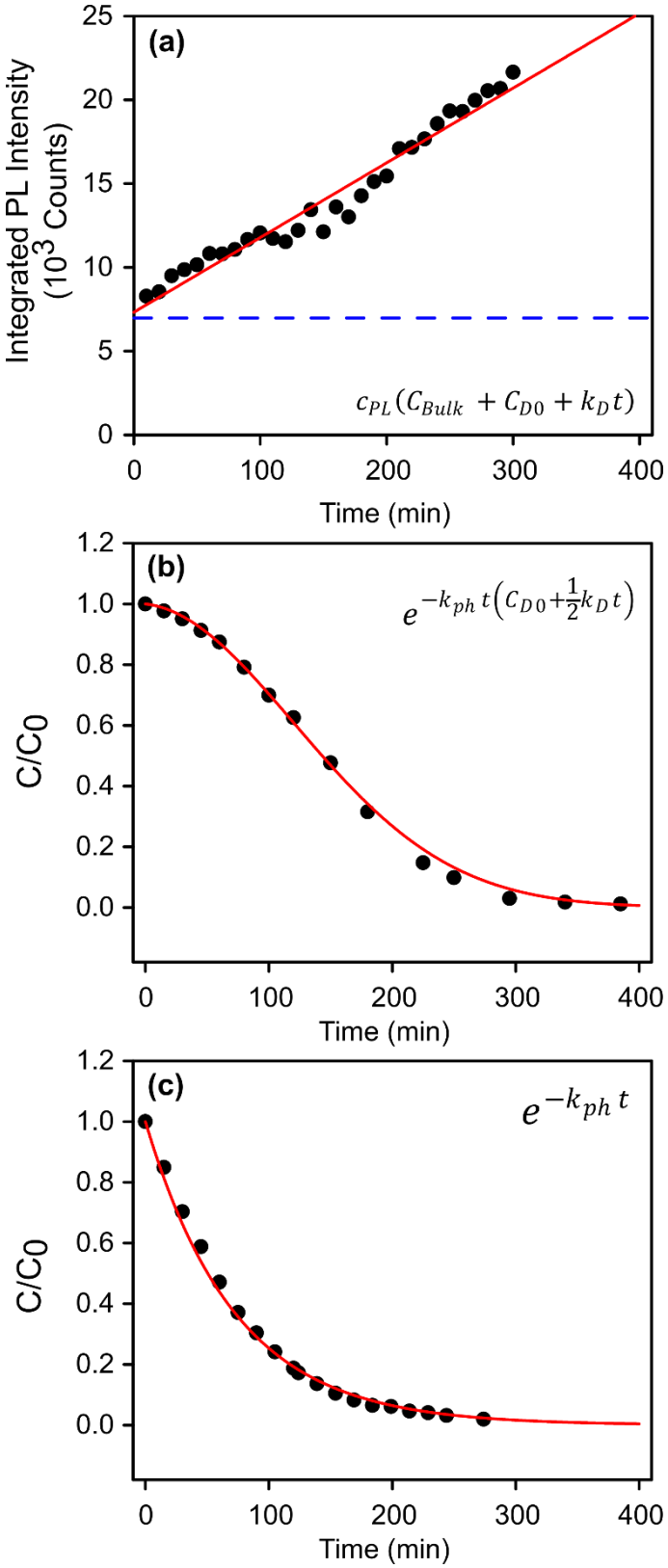

Figure 5: Kinetics data (black points) and relative fitting result (red lines) of (a) photoluminescence intensity, the reference dashed line represents the signal from bulk nanoparticles: $c_{PL} \cdot C_{Bulk}$, (b) 1st cycle photocatalytic experiment, and (c) 2nd cycle photocatalytic experiment.

Reference

1. G. Singh, M. Sharma and R. Vaish, *Chemical Engineering Journal*, 2020, DOI: 10.1016/j.cej.2020.126971, 126971

doi: 10.1016/j.cej.2020.126971

2. H. S. Kushwaha, P. Thomas and R. Vaish, *Journal of Photonics for Energy*, 2017, **7**, 016502

doi: 10.1117/1.Jpe.7.016502

3. S. R. Kadam, R. P. Panmand, R. S. Sonawane, S. W. Gosavi and B. B. Kale, *RSC advances*, 2015, **5**, 58485-58490

doi: 10.1039/C5RA10244H

4. J. Fu, *Materials Letters*, 2012, **68**, 419-422

doi: 10.1016/j.matlet.2011.11.016

5. V. P. Singh and R. Vaish, *Journal of the American Ceramic Society*, 2018, **101**, 2901-2913

doi: 10.1111/jace.15449

6. G. Singh, S. Kumar, V. Singh and R. Vaish, *Journal of Applied Physics*, 2019, **125**, 175102

doi: 10.1063/1.5081988

7. S. Kumar, H. S. Kushwaha, V. P. Singh, R. Vaish, B. Ilahi and N. A. Madhar, *International Journal of Applied Glass Science*, 2018, **9**, 480-486

doi: 10.1111/ijag.12355

8. A. Zandona, A. Martinez Arias, M. Gutbrod, G. Helsch, A. P. Weber and J. Deubener, *Advanced Functional Materials*, 2021, **31**, 2007760

doi: 10.1002/adfm.202007760

9. M. Rastogi, A. Chauhan, H. S. Kushwaha, R. V. Kumar and R. Vaish, *Applied Physics Letters*, 2016, **109**, 223901

doi: 10.1063/1.4970774

10. G. Singh, M. Sharma and R. Vaish, *Communications Materials*, 2020, **1**, 1-8

doi: 10.1038/s43246-020-00101-2

11. J. Xue, X. Wang, J. H. Jeong and X. Yan, *Chemical Engineering Journal*, 2020, **383**, 123082

doi: 10.1016/J.Cej.2019.123082

12. S. K. Apte, S. N. Garaje, S. D. Naik, R. P. Waichal, J.-O. Baeg and B. B. Kale, *Nanoscale*, 2014, **6**, 908-915

doi: 10.1039/C3NR04898E

13. G. Singh, S. Kumar, M. Sharma and R. Vaish, *Journal of the American Ceramic Society*, 2019, **102**, 5127-5137

doi: 10.1111/jace.16395

14. C. Shen, Y. Wang, J. Xu and G. Luo, *Chemical Engineering Journal*, 2012, **209**, 478-485

doi: 10.1016/j.cej.2012.08.044

15. W. Holand and G. H. Beall, *Glass-ceramic technology*, John Wiley & Sons, 2019.

16. L. R. Pinckney and G. H. Beall, 2001

doi: 10.1117/12.446883

17. N. Golubev, E. Ignat'eva, V. Sigaev, A. Lauria, L. De Trizio, A. Azarbod, A. Paleari and R. Lorenzi, *Physical Chemistry Chemical Physics*, 2015, **17**, 5141-5150

doi: 10.1039/c4cp05485g
18. T. Suzuki, G. S. Murugan and Y. Ohishi, *Applied Physics Letters*, 2005, **86**, 131903

doi: 10.1063/1.1891272
19. T. Oshima, T. Nakazono, A. Mukai and A. Ohtomo, *Journal of crystal growth*, 2012, **359**, 60-63

doi: 10.1016/j.jcrysgro.2012.08.025
20. T. Wang, A. Layek, I. D. Hosein, V. Chirmanov and P. V. Radovanovic, *Journal of Materials Chemistry C*, 2014, **2**, 3212-3222

doi: 10.1039/C3TC31823K
21. M. Hegde, T. Wang, Z. L. Miskovic and P. V. Radovanovic, *Applied Physics Letters*, 2012, **100**, 141903

doi: 10.1063/1.3698390
22. N. Pinna, G. Garnweitner, M. Antonietti and M. Niederberger, *Journal of the American Chemical Society*, 2005, **127**, 5608-5612

doi: 10.1021/ja042323r
23. H. Hayashi, R. Huang, F. Oba, T. Hirayama and I. Tanaka, *Journal of Materials Research*, 2011, **26**, 578-583

doi: 10.1557/jmr.2010.32
24. D. Kisailus, Q. Truong, Y. Amemiya, J. C. Weaver and D. E. Morse, *Proceedings of the National Academy of Sciences*, 2006, **103**, 5652-5657

doi: 10.1073/pnas.0508488103
25. X. Zhang, Z. Zhang, J. Liang, Y. Zhou, Y. Tong, Y. Wang and X. Wang, *Journal of Materials Chemistry A*, 2017, **5**, 9702-9708

doi: 10.1039/C7TA02043K
26. R. Lorenzi, A. Paleari, N. V. Golubev, E. S. Ignat'eva, V. N. Sigaev, M. Niederberger and A. Lauria, *Journal of Materials Chemistry C*, 2015, **3**, 41-45

doi: 10.1039/C4TC02118E
27. C. O. Areán, A. L. Bellan, M. P. Mentruit, M. R. Delgado and G. T. Palomino, *Microporous and mesoporous materials*, 2000, **40**, 35-42

doi: 10.1016/S1387-1811(00)00240-7
28. Y. Hou, L. Wu, X. Wang, Z. Ding, Z. Li and X. Fu, *Journal of Catalysis*, 2007, **250**, 12-18

doi: 10.1016/j.jcat.2007.05.012
29. X. Zhang, H. Huang, Y. Zhang, D. Liu, N. Tong, J. Lin, L. Chen, Z. Zhang and X. Wang, *ACS omega*, 2018, **3**, 14469-14476

doi: 10.1021/acsomega.8b01964
30. V. Ghodsi, S. Jin, J. C. Byers, Y. Pan and P. V. Radovanovic, *The Journal of Physical Chemistry C*, 2017, **121**, 9433-9441

doi: 10.1021/acs.jpcc.7b02275
31. V. N. Sigaev, N. V. Golubev, E. S. Ignat'eva, B. Champagnon, D. Vouagner, E. Nardou, R. Lorenzi and A. Paleari, *Nanoscale*, 2013, **5**, 299-306

doi: 10.1039/C2NR32790B
32. V. N. Sigaev, N. V. Golubev, E. S. Ignat'eva, A. Paleari and R. Lorenzi, *Nanoscale*, 2014, **6**, 1763-1774

doi: 10.1039/c3nr05210a
33. S. Lotarev, A. Lipatiev, N. Golubev, E. Ignat'eva, G. Malashkevich, A. Mudryi, Y. S. Priseko, R. Lorenzi, A. Paleari and V. Sigaev, *Optics letters*, 2013, **38**, 492-494

doi: 10.1364/OL.38.000492
34. N. Golubev, E. Ignat'eva, V. Mashinsky, E. Kozlova, V. Sigaev, A. Monguzzi, A. Paleari and R. Lorenzi, *Journal of Non-Crystalline Solids*, 2019, **515**, 42-49

doi: 10.1016/j.jnoncrysol.2019.04.006
35. V. Sigaev, N. Golubev, E. Ignat'eva, V. Savinkov, M. Campione, R. Lorenzi, F. Meinardi and A. Paleari, *Nanotechnology*, 2011, **23**, 015708

doi: 10.1088/0957-4484/23/1/015708
36. V. M. Mashinsky, N. M. Karatun, V. A. Bogatyrev, V. N. Sigaev, N. V. Golubev, E. S. Ignat'eva, R. Lorenzi, M. C. Mozzati, A. Paleari and E. M. Dianov, *Microscopy and Microanalysis*, 2012, **18**, 259-265

doi: 10.1017/S1431927611012827
37. J. Remondina, S. Trabattoni, A. Sassella, N. V. Golubev, E. S. Ignat'eva, V. N. Sigaev, M. Acciarri, B. Schrode, R. Resel and A. Paleari, *Materials & Design*, 2021, **204**, 109667

doi: 10.1016/J.Matdes.2021.109667
38. N. Golubev, E. Ignat'eva, V. Sigaev, L. De Trizio, A. Azarbod, A. Paleari and R. Lorenzi, *Journal of Materials Chemistry C*, 2015, **3**, 4380-4387

doi: 10.1039/c4tc02837f
39. A. Marotta, A. Buri and F. Branda, *Journal of materials science*, 1981, **16**, 341-344

doi: 10.1007/Bf00738622
40. A. Marotta, S. Saiello, F. Branda and A. Buri, *Thermochimica Acta*, 1981, **46**, 123-129

doi: 10.1016/0040-6031(81)80237-7
41. L. Binet and D. Gourier, *Journal of Physics and Chemistry of Solids*, 1998, **59**, 1241-1249

doi: 10.1016/S0022-3697(98)00047-X
42. J. Schneider, M. Matsuoka, M. Takeuchi, J. Zhang, Y. Horiuchi, M. Anpo and D. W. Bahnemann, *Chemical reviews*, 2014, **114**, 9919-9986

doi: 10.1021/cr5001892
43. K. V. Kumar, K. Porkodi and F. Rocha, *Catalysis Communications*, 2008, **9**, 82-84

doi: 10.1016/j.catcom.2007.05.019
44. V. Ghodsi, W. Lu and P. V. Radovanovic, *The Journal of Physical Chemistry C*, 2018, **123**, 433-442

doi: 10.1021/acs.jpcc.8b08613
45. *Journal*

doi:
46. A. Paleari, V. Sigaev, N. Golubev, E. Ignat'eva, S. Bracco, A. Comotti, A. Azarbod and R. Lorenzi, *Acta Materialia*, 2014, **70**, 19-29

doi: 10.1016/j.actamat.2014.02.022
47. S. Jin, W. Lu, P. C. Stanish and P. V. Radovanovic, *Chemical Physics Letters*, 2018, **706**, 509-514

doi: 10.1016/j.cplett.2018.06.046
48. Y. Takano, Y. Hayashi, J. Fukushima and H. Takizawa, *Advanced Powder Technology*, 2021, **32**, 860-865

doi: 10.1016/j.apt.2021.01.032
49. G. McVay and C. Buckwalter, *Nuclear Technology*, 1980, **51**, 123-129

doi: 10.13182/Nt80-A32590
50. S. Ohira and N. Arai, *physica status solidi c*, 2008, **5**, 3116-3118

doi: 10.1002/pssc.200779223
51. J. C. Lapp and J. E. Shelby, *Journal of the American Ceramic Society*, 1987, **70**, 271-274

doi: 10.1111/j.1151-2916.1987.tb04980.x
52. R. Conradt, *Journal of the American Ceramic Society*, 2008, **91**, 728-735

doi: 10.1111/j.1551-2916.2007.02101.x
53. M. D. McCluskey, *Journal of Applied Physics*, 2020, **127**, 101101

doi:
54. T. Wang, S. S. Farvid, M. Abulikemu and P. V. Radovanovic, *Journal of the American Chemical Society*, 2010, **132**, 9250-9252

doi: 10.1021/ja101333h
55. J. R. Lakowicz, *Principles of fluorescence spectroscopy*, Springer science & business media, 2013.
56. W. Z. Tang and H. An, *Chemosphere*, 1995, **31**, 4157-4170

doi: 10.1016/0045-6535(95)80015-D
57. A. Testino, I. R. Bellobono, V. Buscaglia, C. Canevali, M. D'Arienzo, S. Polizzi, R. Scotti and F. Morazzoni, *Journal of the American Chemical Society*, 2007, **129**, 3564-3575

doi: 10.1021/ja067050+
58. R. Scotti, I. R. Bellobono, C. Canevali, C. Cannas, M. Catti, M. D'Arienzo, A. Musinu, S. Polizzi, M. Sommariva and A. Testino, *Chemistry of Materials*, 2008, **20**, 4051-4061

doi: 10.1021/cm800465n

Supporting Information

TEM characterization:

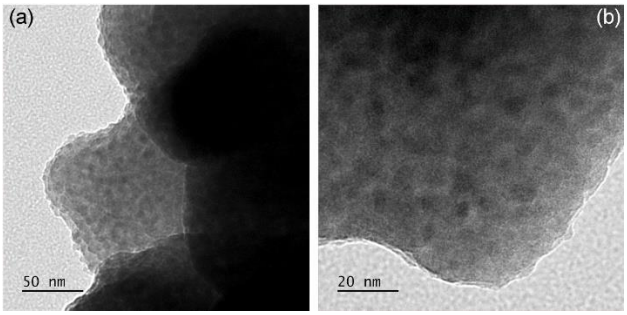

Fig. S1: Representative TEM images of the thermally treated glassceramic.

Phenol degradation:

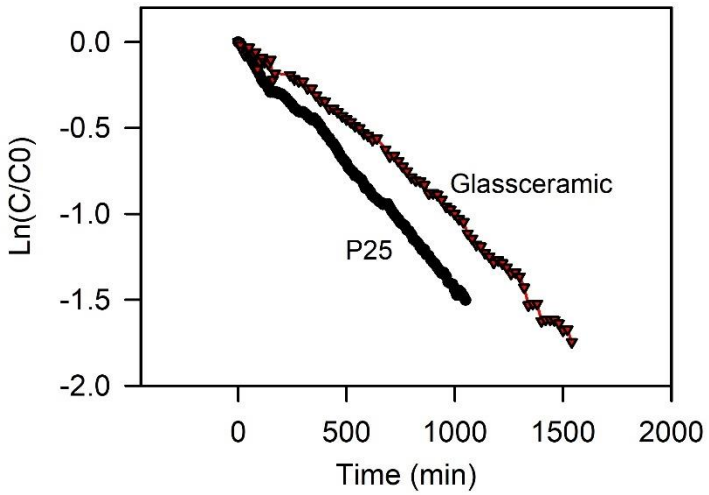

Fig. S2: Photocatalytic experiment on phenol using 1.6 mg of commercial P25 (black circles) and 20 mg of glassceramics (red triangles). The absorption peak at 270 nm has been used to monitor phenol concentration.

Photocatalytic activity of 2 µm sized grains:

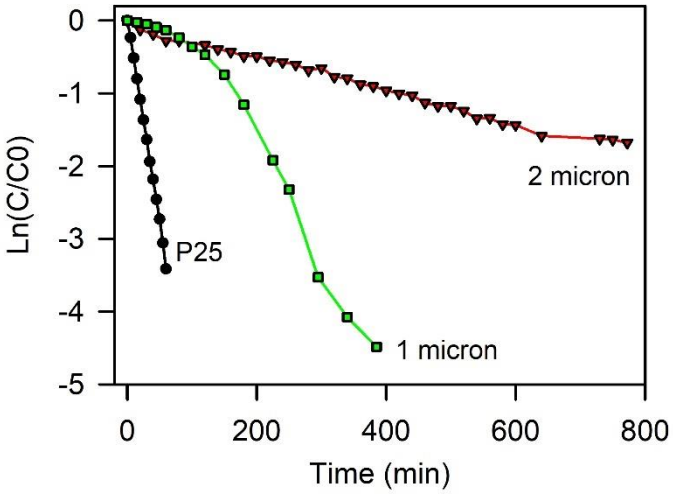

Fig. S3: Comparison of photocatalytic experiment on rhodamine using 1.6 mg of commercial P25 (black circles), 32 mg of glassceramics with grain size of about 1 µm (green squares) and 37 mg of grains with a size of about 2 µm (red triangles).

Photocatalytic activity after rest in water

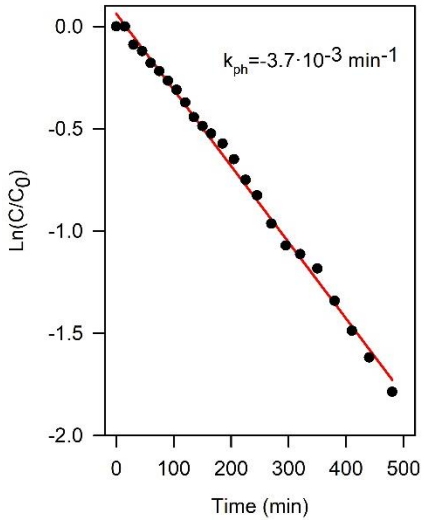

Fig. S4: Photocatalytic experiment after leaving the powdered glass-ceramic 8 hours in water.

XRF analysis:

	Ge (%mol)	Ga (%mol)	Zr (%mol)
Before rest in water	45.0±0.1	19.5±0.1	1.5±0.1
After rest in water	45.0±0.1	19.4±0.1	1.4±0.1

Tab. S1: XRF analysis of the main component of amorphous matrix, crystalline phase, and impurities due to ball-milling contamination. Data refer to analysis conducted before and after 12 h of rest in water.

XRD analysis:

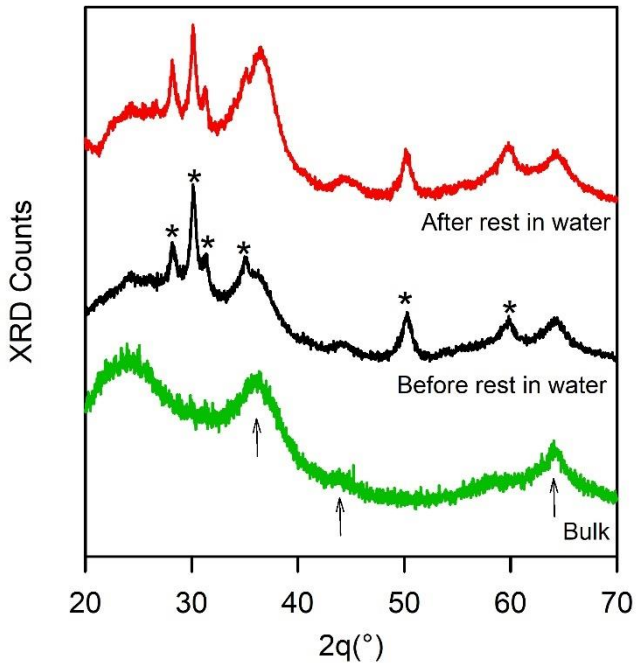

Fig. S5: XRD patterns of the glassceramic bulk (green line) and powdered samples before (black line) and after (red line) 12 h of rest in water. Arrows indicate main reflections from Ga_2O_3 in the gamma phase (PDF file: 00-020-0426) and asterisks indicate reflections from ZrO_2 (PDF file: 00-002-0733) contamination during prolonged ball-milling.

Lifetime fitting procedure:

Time resolved photoluminescence data have been fitted considering deconvolution with the Instrument Response Function (IRF). The temporal profile of IRF has been assumed to be Gaussian in shape:

$$IRF(t) = a_{IRF}\frac{e^{-\frac{(t-t_0)^2}{2{w_t}^2}}}{\sqrt{2\pi}w_t} \quad Eq.(S1)$$

Where a_{IRF}, t_0, and w_t are the amplitude, the position of the peak maximum and the standard deviation of the IRF. The fitting of the IRF is reported in Fig. S1, with fitting results of a_{IRF} = 13142, t_0 = 15.13 ns and w_t = 0.675 ns.

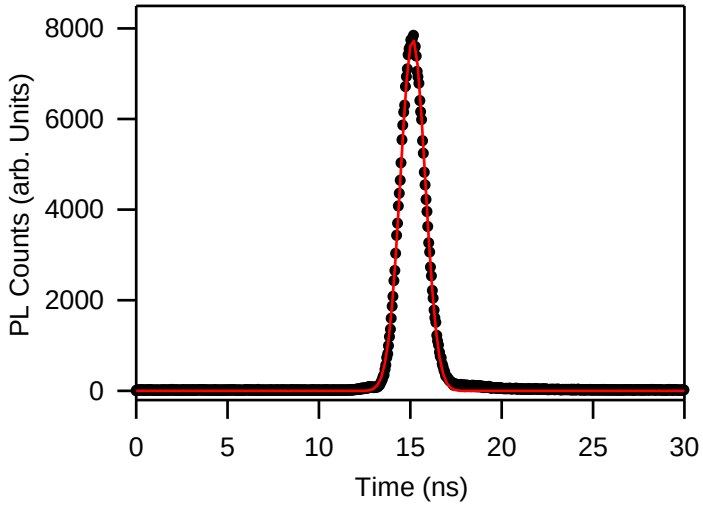

Fig. S6: Instrument Response Function of the pump laser used for time-resolved photoluminescence (black points) and Gaussian fit (red line)

The same function has been used to calculate the convolution with a triple exponential:

$$I(t) = (f * g)(t) \coloneqq \int_0^t f(\tau)\, g(t-\tau)d\tau = \int_0^t \left(\sum_{i=1}^{3} a_i e^{-\frac{\tau}{\tau_i}}\right)\left(\frac{e^{-\frac{(t-\tau-t_0)^2}{2{w_t}^2}}}{\sqrt{2\pi}w_t}\right)d\tau \quad Eq.(S2)$$

Which has the following solution:

$$I(t) = c + \sum_{i=1}^{n}\frac{1}{2}a_i e^{\frac{{w_t}^2-2\tau_i(2t_0+t)}{2{\tau_i}^2}}\left(\mathrm{erf}\left[\frac{{w_t}^2+t_0\tau_i}{\sqrt{2}w_t\tau_i}\right]-\mathrm{erf}\left[\frac{{w_t}^2+(t_0-t)\tau_i}{\sqrt{2}w_t\tau_i}\right]\right) \quad Eq.(S3)$$

Where the fitting parameters are c, a_i, and τ_i are a constant which takes into account the signal background, the amplitude, and the time constant of the i-th lifetime contribution, respectively.

Time-resolved photoluminescence data:

Time (min)	c	a_1	a_2	a_3	τ_1 (ns)	τ_2 (ns)	τ_3 (ns)
0	88.6	3350	267.4	74.7	0.107	2.5	14.5
10	61.9	3053	282.9	69.8	0.121	2.6	17.7
20	62.4	3073	303.3	83.7	0.128	2.6	16.4
30	69.1	3181	322.7	78.7	0.137	2.8	19.3
40	73.5	3332	329.8	88.7	0.123	2.6	17.5
50	75.5	3366	327.9	88.7	0.125	2.6	18.6
60	80.6	3362	330.2	88.5	0.128	2.8	19.8
70	80.8	3278	356.2	91.2	0.128	2.5	19.3
80	82.2	3523	325.3	89.4	0.129	2.9	20.0
90	88.5	3218	349.9	100.3	0.135	2.6	18.4
100	91.7	3598	355.8	91.7	0.120	2.7	21.1
110	88.6	3788	374.3	93.2	0.127	2.6	19.1
120	86.8	3105	314.0	88.1	0.139	3.0	21.2
130	93.6	3230	332.2	101.3	0.133	2.7	18.8
140	105.1	3447	323.2	101.9	0.130	2.9	19.8
150	93	3151	335.1	97.7	0.139	2.6	19.1
160	107.2	3622	331.3	103.5	0.126	2.8	19.2
170	103.6	4083	394.8	113.0	0.100	2.1	16.7
180	112.9	3679	384.1	102.3	0.120	2.6	19.9
190	118.3	3688	356.9	98.7	0.132	3.0	22.7
200	123.2	3747	355.2	111.7	0.124	2.7	19.9
210	136.8	3847	424.9	120.0	0.121	2.5	20.4
220	138.9	3430	392.7	121.4	0.130	2.5	20.0
230	142.4	3377	378.4	115.4	0.138	2.8	21.9
240	149.8	3447	397.9	129.5	0.136	2.6	21.1
250	157.3	3551	404.0	121.6	0.130	2.8	22.6
260	157.7	3528	405.6	130.6	0.130	2.5	20.9
270	163.9	3485	401.4	120.4	0.135	2.8	22.4
280	169	3474	381.6	121.5	0.138	2.9	23.1
290	169.8	3339	387.1	123.6	0.140	2.9	23.1
300	178.7	3415	396.1	116.6	0.138	3.1	24.6

Tab. S2: Fitting results of time-resolved photoluminescence experiment. The fitting function is given in Eq.(S3).

Plot of $\langle\tau\rangle/I$ as a function of time

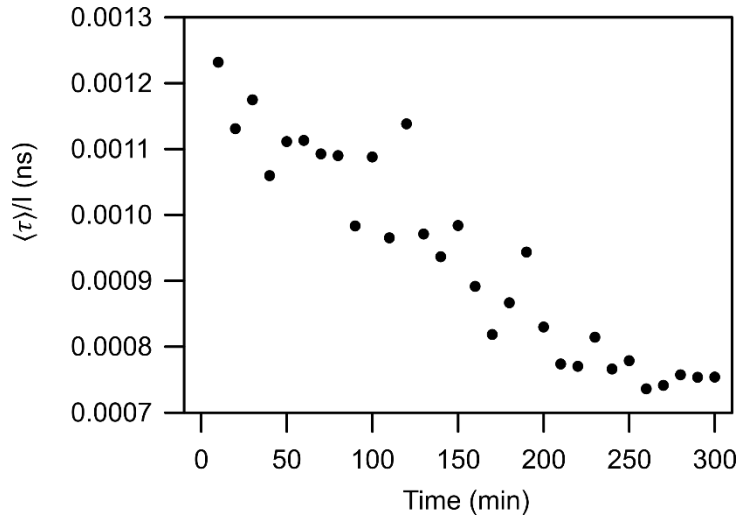

Fig. S7: Ratio of the mean lifetime over the integrated intensity from time-resolved photoluminescence as a function of the time in water spent by the glassceramic powder.

Fitting results of kinetics:

Parameter	Fitted value
k_{ph} [min^{-1}]	1.35·10-3
C_{D0}	3.06·10-2
k_D [min^{-1}]	4.76·10-3
c_{PL}	9378
C_{Bulk}	0.75

Tab. S2: Fitting results of kinetic experiments, the fitting functions are reported in the main text (Eq. 8).